ACS APPLIED MATERIALS & INTERFACES

Research Article

www.acsami.org

Facile Synthesis and Lithium Storage Properties of a Porous $NiSi_2$/Si/Carbon Composite Anode Material for Lithium-Ion Batteries

Haiping Jia, Christoph Stock, Richard Kloepsch, Xin He, Juan Pablo Badillo, Olga Fromm, Britta Vortmann, Martin Winter,* and Tobias Placke*

MEET Battery Research Center, Institute of Physical Chemistry, University of Münster, Corrensstrasse 46, 48149 Münster, Germany

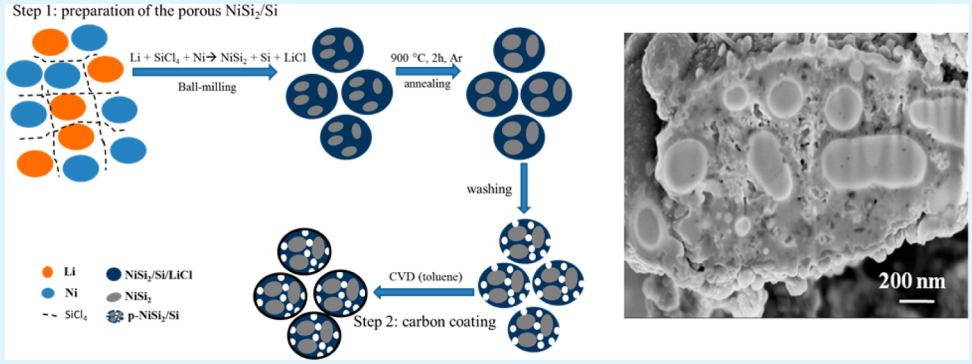

ABSTRACT: In this work, a novel, porous structured $NiSi_2$/Si composite material with a core−shell morphology was successfully prepared using a facile ball-milling method. Furthermore, the chemical vapor deposition (CVD) method is deployed to coat the $NiSi_2$/Si phase with a thin carbon layer to further enhance the surface electronic conductivity and to mechanically stabilize the whole composite structure. The morphology and porosity of the composite material was evaluated by scanning electron microscopy (SEM), transmission electron microscopy (TEM), and nitrogen adsorption measurements (BJH analysis). The as-prepared composite material consists of $NiSi_2$, silicon, and carbon phases, in which the $NiSi_2$ phase is embedded in a silicon matrix having homogeneously distributed pores, while the surface of this composite is coated with a carbon layer. The electrochemical characterization shows that the porous and core−shell structure of the composite anode material can effectively absorb and buffer the immense volume changes of silicon during the lithiation/delithiation process. The obtained $NiSi_2$/Si/carbon composite anode material displays an outstanding electrochemical performance, which gives a stable capacity of 1272 mAh g^{-1} for 200 cycles at a charge/discharge rate of 1C and a good rate capability with a reversible capacity of 740 mAh g^{-1} at a rate of 5C.

KEYWORDS: *$NiSi_2$/Si composite, anode material, porous structure, ball milling, lithium-ion batteries*

1. INTRODUCTION

Currently, lithium-ion batteries (LIBs) have drawn worldwide attention since they are one of the most important energy storage devices for portable electronics and also intensively considered as storage systems for electric vehicles and stationary energy storage.[1−3]

Regarding the current need for high-capacity anode materials in order to further increase the specific energy (Wh kg^{-1}) and energy density (Wh L^{-1}) of LIBs, silicon is one of the most promising candidates. Among different alloying elements, such as tin or aluminum, silicon displays the highest theoretical capacity of 4200 mAh g^{-1} (practical ca. 3500 mAh g^{-1}) and a relatively low lithiation potential of 0.2 V vs Li/Li^+, compared to the conventional carbonaceous anode materials, displaying a relatively low specific capacity (372 mAh g^{-1}), which cannot meet the growing demand for the next-generation high-performance lithium-ion batteries. However, there are some critical drawbacks arising with the use of silicon, which are mainly related to the severe volume changes (up to 300%) during the lithium insertion/extraction process and the low intrinsic electronic conductivity.[4−7] The large stress and strain during lithiation/delithiation may lead to particle cracking and even particle pulverization. The volume changes of alloying materials in general also lead to a contact loss between the active material particles and the conductive carbon and/or current collector as well as to an ongoing formation of the solid electrolyte interphase (SEI; dynamic process of breaking off and reforming) and an increase in the overall resistance, thus resulting in an enhanced capacity fading during charge/discharge cycling.[8−11]

Several strategies have been developed in order to reduce the detrimental effects of the large volume changes of silicon and to suppress the side reactions with the electrolyte and thus to improve the long-term cycling stability.[8] One main approach is

Received: September 22, 2014
Accepted: January 9, 2015
Published: January 9, 2015

DOI: 10.1021/am506486w
ACS Appl. Mater. Interfaces 2015, 7, 1508−1515

to reduce the silicon particle size to the nanometer range, while several material structures, including, e.g., nanowires,[12] nanospheres,[13] and nanotubes,[14] have been proposed. In addition, another strategy is to design porous structures, e.g., macroporous (pore width > 50 nm) or mesoporous materials (pore width of 2−50 nm), that can offer sufficient local void space to absorb the volume expansion of silicon and thus enhance the cycling stability.[15−18]

A further main strategy to improve the electrochemical performance of silicon is the formation of multiphase composite materials, i.e., by introducing a second or more components, which display no or only less volume changes as well as preferentially a high electronic conductivity. The idea of this approach is to use the host matrix to buffer the volume changes of silicon and thus to maintain the electrode integrity and electronic network. Examples are silicon−carbon composite materials, e.g., silicon particles dispersed in a carbon composite matrix,[19,20] and silicon-based alloys or composite heterostructures, such as Si/SiO_x/carbon composites,[21,22] or intermetallic compounds like Si/$TiSi_2$[23] or NiSi alloys.[24,25]

For example, Chen et al. synthesized a $FeSi_2$/Si@C composite material using a ball-milling procedure, which showed a reversible capacity of 1010 mAh g^{-1} and an excellent cycling stability with 94% capacity retention after 200 cycles.[26] In recent years, several reports on the topic of $NiSi_x$ phases appeared in the literature. Fan et al. adopted two steps of CVD processes to obtain ordered Ni_3Si_2/Si nanorod arrays to decrease the tendency of active particle pulverization.[27] The material exhibited an excellent cycling performance at high current rates. A high and steady discharge capacity of more than 2184 mA h g^{-1} could be achieved after 50 cycles with a high initial Coulombic efficiency of 86.7%. However, the complicated and high-cost synthesis process hinders its large-scale production.[27] Furthermore, Liu et al. synthesized a nanoporous NiSi/Si composite anode material via a facile ball-milling method.[24] Nevertheless, this material presented a relatively strong capacity fading over 50 charge/discharge cycles. Kim et al. prepared a core−shell Si/$NiSi_2$/carbon composite material via heat treatment of a mixture of silicon powder and nickel phthalocyanine.[28] The cycling performance over 50 cycles was improved, compared to bare silicon, but still displayed a remarkable capacity fading. However, the specific capacity was decreased to only 800 mAh g^{-1} at a rate of 0.1C. The relatively poor cycling stability as well as a poor rate capability of this material may be related to the fact that the amount of the $NiSi_2$ phase was not high enough to buffer the volume changes of silicon and/or the solid structure was not favorable, i.e., did not show a sufficient porosity, for a fast transport of Li^+. Even though all of the above-mentioned attempts brought significant improvements regarding the electrochemical performance or production costs of silicon-based anode materials, these techniques still cannot meet the requirements for an industrial application due to the unsatisfactory comprehensive performance of the resulting materials and/or high costs for mass production.[24]

In this work, we report a facile synthesis route for a porous core−shell $NiSi_2$/Si/carbon composite material and its electrochemical characterization as anode material for lithium-ion batteries. The simple and high-yield synthesis process, using cheap and abundant raw materials, makes it more competitive for industrial applications. The obtained anode material demonstrates an adequate distribution in which $NiSi_2$ particles are surrounded by silicon crystallites. Furthermore, a chemical vapor deposition (CVD) method is deployed to coat the $NiSi_2$/Si phase to further enhance the surface electronic conductivity and stabilize the whole structure. As a result, the synthesized $NiSi_2$/Si/carbon composite displays excellent electrochemical performance, i.e., a good cycling stability and charge/discharge rate performance.

2. EXPERIMENTAL SECTION

2.1. Preparation of the Porous $NiSi_2$/Si Composite Material. First, high-purity metallic lithium sheets (Rockwood Lithium; purity, battery grade) were cut into pieces for use. Then, 0.5 g of Li, 0.168 g of Ni (Sigma-Aldrich; purity 99.9%), and 3 mL of $SiCl_4$ (Sigma-Aldrich; purity 99%) were mixed in an 80 mL argon-filled zirconium vial with 15 zirconium balls of 10 mm in diameter and ball milled in a 350 rotations/min high-energy mechanical mill for 20 h. The product was transferred into a quartz tube, followed by a heat treatment at 900 °C for 2 h in argon atmosphere. The obtained gray powder was immersed in distilled water for 12 h and then washed with ethanol and distilled water by centrifugation for 4 times. By this process, LiCl was removed and porous $NiSi_2$/Si was obtained.

2.2. Fabrication of Carbon-Coated Porous $NiSi_2$/Si. The $NiSi_2$/Si composite material was coated with carbon via a chemical vapor deposition (CVD) method using toluene as the carbon source and argon as carrier gas. The $NiSi_2$/Si was put into a quartz tube furnace and first flushed with argon for 30 min to flush away any oxygen in the reactor. Then, the temperature of the furnace was increased to 800 °C and kept at this temperature for 1 h under argon and toluene mixed atmosphere flow (5 L h^{-1}, 10 mL of toluene was used for carbon coating within 1 h). After carbon coating, the furnace was cooled to room temperature. The resulting composite was designed as $NiSi_2$/Si-carbon composite.

2.3. Structure and Morphology Characterization. X-ray diffraction (XRD) measurements were carried out using a Bruker D8 Advance X-ray diffractometer (Bruker AXS GmbH) equipped with a copper target X-ray tube (radiation wavelength λ = 0.154 nm).

In situ XRD analysis of the $NiSi_2$/Si/carbon anode material upon galvanostatic lithiation and delithiation was performed by using a self-designed in situ cell, whose design has been inspired by earlier reports.[29−31] The electrode stack is electrically insulated from the stainless steel body by a sheet of Mylar foil. The electrode paste was cast on a beryllium (Be) window, which served as both the current collector and the "window" for the X-ray beam, to analyze the structure changes during the lithiation and delithiation processes of the $NiSi_2$/Si/carbon active material. The coated Be window was subsequently dried at 80 °C for 30 min in air and at 40 °C under vacuum (<0.1 mbar) for 12 h. Metallic lithium foil served as counter electrode. Whatman glass fiber (grade GF/D) served as separator, drenched with 500 μL of 1 M $LiPF_6$ in EC:DEC 3:7 (in weight ratio), plus 10 wt % FEC. The assembled cell was allowed to rest for 6 h to ensure a sufficient wetting of the electrode. Subsequently, the cell was galvanostatically cycled at a specific current of 0.05C to a complete initial discharge (lithiation) to 0.01 V, for approximately 20 h. In parallel, XRD patterns were acquired in an angular range from 20° to 80°, with a step size of 0.02239° and a time per step of 0.4 s, resulting in a complete scan for every 20 min. After discharging to a lower cutoff voltage of 0.01 V, the cell was charged (delithiation) to an upper cutoff voltage of 1.5 V.

The morphology of the samples was studied by a field emission scanning electron microscope (Carl Zeiss AURIGA, Carl Zeiss Microscopy GmbH). Transmission electron microscopy (TEM, JEOL JEM-100CX) was used to investigate the microstructures of the $NiSi_2$/Si and the $NiSi_2$/Si/carbon composites. A focused-ion beam (FIB-SEM) study was carried out to investigate the interior of the composite material.

The BET specific surface area and BJH pore diameter distribution have been determined by nitrogen adsorption measurements using an ASAP 2020 (Accelerated Surface Area and Porosimetry Analyzer, Micromeritics GmbH). Before the measurement, the samples were

DOI: 10.1021/am506486w
ACS Appl. Mater. Interfaces 2015, 7, 1508−1515

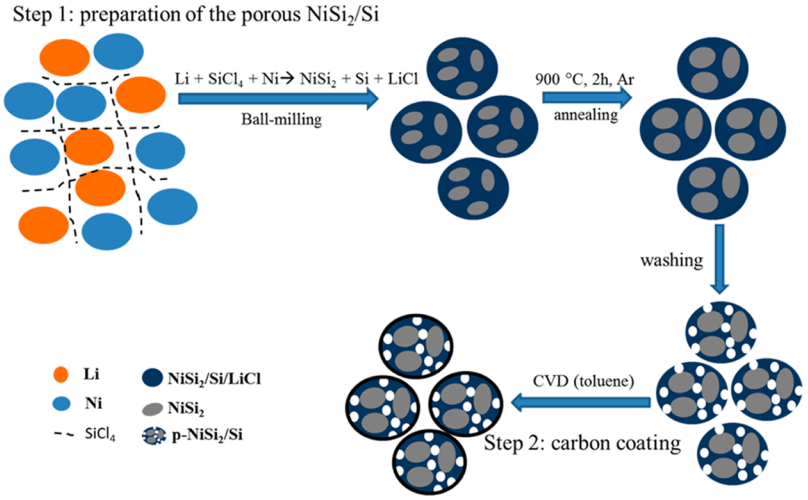

Figure 1. Schematic illustration of the preparation process of the porous $NiSi_2$/Si/carbon composite material.

degassed at 120 °C until a static pressure of less than 0.01 Torr (0.0133 mbar) was reached.

The purity and Ni:Si ratio of the composite material were analyzed by inductively coupled plasma-optical emission spectrometry (ICP-OES). Prior to the investigation, the samples were digested with HCl/HNO_3 (1:1) in a microwave (Multiwave 3000 solv, Anton Paar, Austria), then filled up to 50 mL with Milli-Q water. The analysis itself was carried out on a Spectro ARCOS ICP-OES (Spectro Analytical Instruments, Kleve, Germany) instrument with axial plasma viewing determining the ratio of Ni:Si of the sample (used wavelengths Si 251.612, 288.158, 212.412 nm; Ni 231.604, 221.648, 227.021, 174.828 nm).

Thermogravimetric analysis (TGA) was conducted using a TGA Q5000 IR system (TA Instruments). The measurements were carried out in oxygen atmosphere in the temperature range from 30 to 1000 °C with a heating rate of 10 °C min^{-1}.

2.4. Electrode Preparation, Cell Assembly, and Electrochemical Investigations. Composite electrodes were prepared using a composition of 70 wt % active material, 15 wt % of conductive carbon black agent C-nergy Super C65 (Imerys Graphite & Carbon), and 15 wt % of sodium carboxymethylcellulose (CMC, Walocel CRT 2000 PA 12) as binder. Prior to the dispersion of the solid compounds, the binder polymer was dissolved in deionized water to obtain a 2.0 wt % solution. An appropriate amount of Super C65 was added to the binder solution, and the mixture was further homogenized by stirring. Afterward, a high-energy dispersion step (Ultra-Turrax T25, 1 h, 5000 rpm) was deployed to eliminate agglomerates and homogenize the mixture. The paste was cast on a copper foil by a standard lab-scale doctor-blade technique. The gap of the doctor blade was set to 120 μm wet film thickness, leading to an average mass loading of 1.08 mg cm^{-2}. After casting, the tapes were transferred into an oven and dried in air for 1 h at 80 °C. Electrodes with a diameter of 12 mm were cut out, and a further drying step was performed under an oil-pump vacuum (<0.1 mbar) at 120 °C for 24 h. Thereafter, the electrodes were stored in an argon-filled glovebox (UniLab, MBraun) with water and oxygen contents of less than 1 ppm.

Electrochemical experiments were performed using CR2032-type coin cells with Celgard 2400 as separator and high-purity metallic lithium (Rockwood Lithium) as counter electrode. The electrolyte was 1 M $LiPF_6$ in a mixture of ethylene carbonate (EC) and diethyl carbonate (DEC) (3:7 in weight ratio), plus 10 wt % FEC. The cells were assembled in an argon-filled glovebox with oxygen and water contents of less than 1 ppm. The electrochemical performance was evaluated on a Maccor 4300 battery test system at 20 °C. The cutoff voltage was 0.01 V for the discharge process (lithiation) and 1.2 V for the charge process (delithiation). The specific capacity was calculated on the basis of the total composite weight, and the C rate was calculated with respect to the theoretical capacity of 2300 mAh g^{-1} (1C) for $NiSi_2$/Si and 2034 mAh g^{-1} (1C) for $NiSi_2$/Si/carbon. Cyclic voltammetry (CV; 0.01−1.5 V) was performed with a scan rate of 0.02 mV s^{-1} using a VMP multichannel constant voltage-constant current system (Biologic Science Instrument).

3. RESULTS AND DISCUSSION

Figure 1 gives an overview of the mechanical formation of the porous $NiSi_2$/Si composite material. In the first step, $SiCl_4$ is reduced with metallic lithium to obtain silicon powder, which further reacts with nickel to form the $NiSi_2$/Si composite with a silicon phase surrounding the surface of the $NiSi_2$ cores during the high-energy ball-milling procedure. After that, the as-milled product undergoes a heat treatment at 900 °C for 2 h, followed by a washing process using water and ethanol to remove LiCl, and porous $NiSi_2$/Si was obtained. In the second step, a chemical vapor deposition (CVD) method was deployed to coat the porous $NiSi_2$/Si particles with a thin carbon layer using toluene as carbon source (carbon content of 19.5 wt %) to enhance the electronic conductivity and thus to further improve the electrochemical performance of the composite.

The XRD pattern confirms the formation of the $NiSi_2$/Si composite, as illustrated in Figure 2. After milling, the XRD signals of nickel (JCPDS 04-010-6148) disappeared and, instead, a number of new reflexes emerged at 2θ = 28.6°, 47.5°, 56.3°, 69.5° 76.5°, and 88.6°, reflecting complete conversion of nickel into the $NiSi_2$ phase by the ball-milling

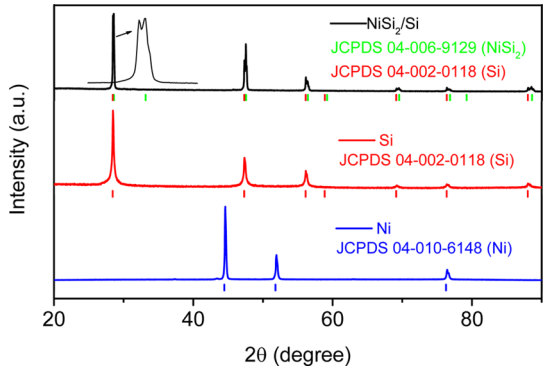

Figure 2. XRD patterns of the $NiSi_2$/Si composite material (black curve), silicon (red curve), and nickel (blue curve). (Inset) Details for 2θ = 28−29°.

DOI: 10.1021/am506486w
ACS Appl. Mater. Interfaces 2015, 7, 1508−1515

and heat treatment conditions. Since the peaks of the $NiSi_2$ (JCPDS 04-006-9129) and silicon (JCPDS 04-002-0118) phase are quite close, the respective part of the pattern is also shown in a higher magnification. As designed with a starting mass ratio of Si:Ni = 3:1, the final ratio of the active silicon and inactive $NiSi_2$ phase in the $NiSi_2$/Si composite is around 1:1, which means that the silicon phase is close to 75.0 wt % in total (Si in the $NiSi_2$ phase is 25 wt %). ICP-OES measurements further confirmed that the mass ratio of silicon and nickel in the composite is 75.0 and 25.0 wt %, respectively, and no LiCl impurities were detected.

The morphology and structure of the $NiSi_2$/Si and the $NiSi_2$/Si/carbon composites is demonstrated by the SEM and TEM measurements in Figures 3 and 4, respectively. Insight into the

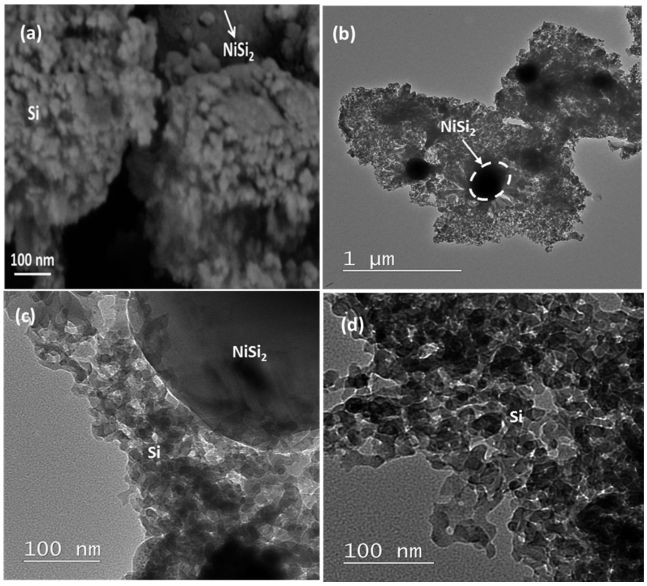

Figure 3. (a) SEM and (b–d) TEM images of the $NiSi_2$/Si composite material.

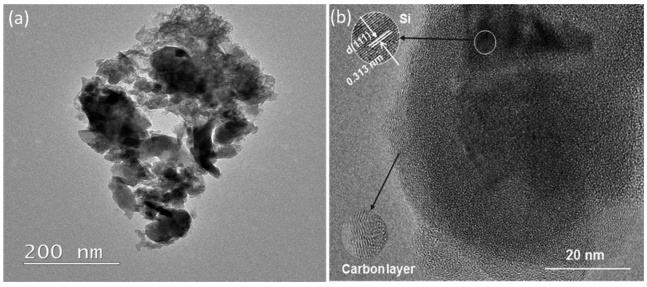

Figure 4. (a) TEM and (b) HR-TEM images of the $NiSi_2$/Si/carbon composite material.

fine structure reveals the open mesoporous character and homogeneous distribution of silicon crystallites with a size of about 20 nm, which are surrounding the surface of the $NiSi_2$ cores (Figure 3). The mesopores are in the range of 20–40 nm with a cumulative pore volume of 0.563 $cm^3\ g^{-1}$ (as shown in the BJH measurement, Figure 5b) and a BET surface area of around 72.6 $m^2\ g^{-1}$, which arise from complete removal of LiCl from the composite (see Figure 1). These pores, having an average size of 25 nm, may effectively accommodate the volume changes of silicon during lithiation/delithiation. Figure 5a depicts the cross-section of a $NiSi_2$/Si particle, obtained by a

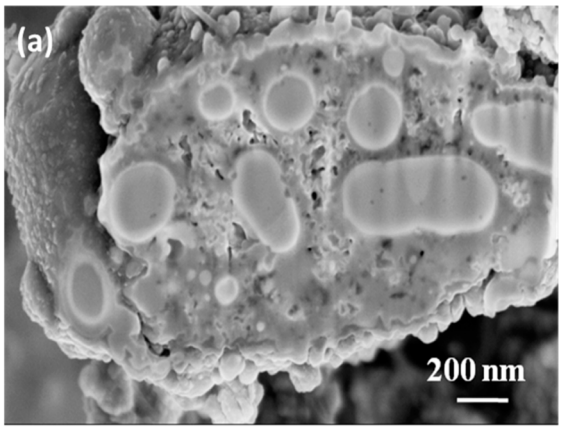

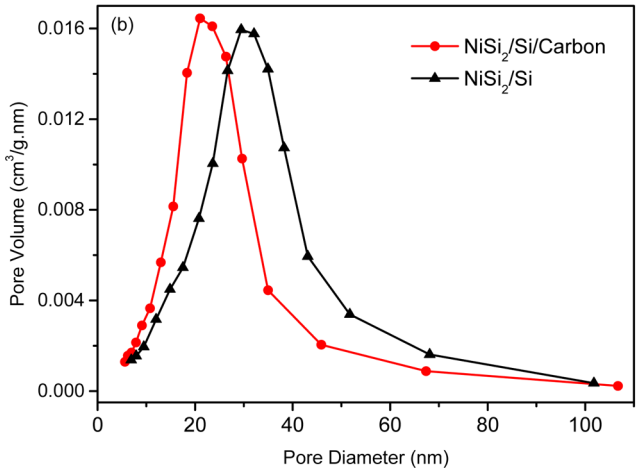

Figure 5. (a) SEM image of the cross-section of a $NiSi_2$/Si composite particle. (b) BJH pore diameter distribution for the $NiSi_2$/Si and $NiSi_2$/Si/carbon composites.

FIB-SEM measurement, and clearly shows the two different phases as well as the existence of a porous structure. A major disadvantage of silicon as electroactive material is its poor electronic conductivity. A surface modification by carbon coating is an appropriate method to improve the electronic conductivity, due to the carbon's low density, low cost, and excellent mixed-conducting property.[20,32] Herein, a CVD method was deployed to cover a thin carbon layer on the surface of $NiSi_2$/Si (see Figure 1). After carbon coating, the average pore size decreases from 25 to 22.4 nm (Figure 5b) due to the carbon deposition within the open pores via the penetration of toluene molecules, which was used as precursor material. The mesoporous structure of the $NiSi_2$/Si/carbon material still brings a high BET specific surface area of 40.8 $m^2\ g^{-1}$, which is favorable for fast electrode kinetics. The HR-TEM image in Figure 4b reveals that the carbon coating layer, covering the surface of the silicon particles, is about 3.5 nm in thickness. One can also clearly see the lattice fringes with an interplanar spacing of 0.3135 nm, corresponding to the Si (111) plane (Figure 4b). In this respect, it is difficult to observe the interplanar spacing of the $NiSi_2$ phase under such a high magnification, due to its relatively large particles. Furthermore, it should be noted that the interplanar spacing of $NiSi_2$ (111) and Si (111) is very close, 0.3121 and 0.3135 nm, respectively. Thus, it is difficult to distinguish the $NiSi_2$ phase from Si according to the interplanar spacing.

DOI: 10.1021/am506486w
ACS Appl. Mater. Interfaces 2015, 7, 1508–1515

The amount of carbon was determined by thermogravimetric analysis, as illustrated in Figure 6. For the $NiSi_2$/Si/carbon

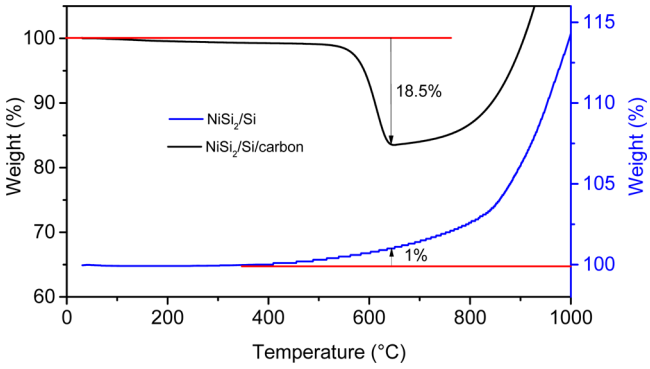

Figure 6. Thermogravimetric analysis of the $NiSi_2$/Si and $NiSi_2$/Si/carbon composites in an oxygen atmosphere in the temperature range from 30 to 1000 °C with a heating rate of 10 °C min^{-1}.

composite, a weight loss was observed from 200 to 600 °C. A rapid mass loss takes place between 450 and 650 °C. At 650 °C, the total mass loss is around 18.5 wt %. For comparison, also the pure $NiSi_2$/Si composite was analyzed at the same conditions. For this material, an increase of the mass from 200 to 600 °C of nearly 1.0 wt % occurs, which is related to the oxidation of the silicon surface. Therefore, the mass percentage ratio of carbon can be estimated to be roughly about 19.5 wt %.

To identify the electrochemical lithiation/delithiation reactions of this composite, cyclic voltammetry (CV) was adopted to measure the $NiSi_2$/Si/carbon composite anode at a scan rate of 0.02 mV s^{-1}. As shown in Figure 7b, the composite displays a constant cathodic current in the first negative scan starting from 1.5 to 0.2 V, due to the irreversible reduction of the organic solvent-based electrolyte and SEI layer formation on the surface of the composite. When the scan proceeds, there is a sharp cathodic peak arising at a low potential of below 0.1 V, which is related to the lithiation and amorphization of silicon.[33] Two broad oxidation peaks appear correspondingly at 0.3 and 0.5 V on the reversed scan, which are characteristic for the reversible lithium extraction reaction with active silicon in the composite.[34] During the second cathodic sweep, a new reduction peak was observed at 0.2 V, which is most likely related to a two-stage alloying reaction of Li^+ with the $NiSi_2$/Si phase with the formation of the two different lithiated states. In addition, two sharp oxidation peaks at 0.3 and 0.5 V appear constantly during the anodic potential sweep. In the case of the fifth and ongoing cycles, an additional reduction peak shows up at around 0.08 V, which corresponds to the formation of another new $LiSi_x$ phase, while the oxidation peaks appear constantly in the same position as before. These results show that the $NiSi_2$/Si electrode demonstrates an activation process within the first 5 cycles and the utilization of silicon is improved after this activation.

The voltage profiles for the constant current charge/discharge cycling of the $NiSi_2$/Si/carbon composite are presented in Figure 7a. In the first cycle, a reversible capacity of 1765 mAh g^{-1} is obtained with a Coulombic efficiency of 81%. The irreversible capacity loss during the first lithiation process can be mainly attributed to the formation of the solid electrolyte interphase (SEI) on the surface of the electrode and the consumption of Li^+ in the composite via structural defects.[35] From the second cycle, the charge/discharge

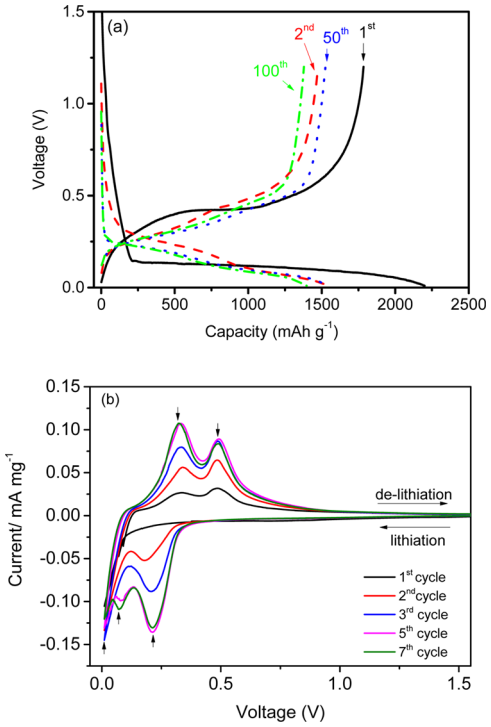

Figure 7. (a) Representative voltage vs specific capacity profiles of the constant current charge/discharge cycling of the $NiSi_2$/Si/carbon composite anode at 0.1C (1st cycle) and 1C (2nd, 50th, and 100th cycle). (b) Differential capacity curves of the 1st (0.1C), 2nd, 3rd, 5th, and 7th (all 1C) cycle of the $NiSi_2$/Si/carbon composite anode.

efficiency increases rapidly to 96% and approaches more than 99% after a few cycles. Meanwhile, the reversible capacity increased from the second cycle to a maximum of 1565 mAh g^{-1}, indicating the existence of an activation process, i.e., an increasing wetting of the electrode and the porous composite structure by the electrolyte.

In order to investigate the electrochemical reaction of the $NiSi_2$/Si composite with lithium, in situ XRD analysis coupled with a constant current lithiation and delithiation process has been carried out (Figure 8). Figure 8a–c display the in situ XRD patterns, while Figure 8d depicts the corresponding voltage profile of the first electrochemical alloying and dealloying reaction. The numbers in Figure 8d correspond to the XRD scan numbers and can be correlated to those in Figure 8a–c. As typically occurring during the discharge (lithiation process), the voltage rapidly dropped to below 0.1 V (Figure 8d). Afterward, several processes were found to take place concurrently. First, the intensity of the silicon peak at 2θ = 28.5° decreased with discharge depth, and it completely disappears at scan 16 (Figure 8b), accompanying with the appearance of Li_xSi phases, as observed in Figure 8a. Second, the intensity of the $NiSi_2$ phase at 2θ = 28.6° also decreases gradually with ongoing lithiation (Figure 8b), but no new Li_xNiSi_2 or Ni_xSi phase could be detected, which is most likely amorphous (Li_xNiSi_2) or the amount is negligible small (Ni_xSi). However, unlike silicon, the peak of the $NiSi_2$ phase does not disappear when the lithiation process ends. During the charge (delithiation) process, the Li_xSi phases disappear as the charge process continues, and the crystalline silicon phase does not reappear as its structure remains amorphous and is hence not detectable by XRD. Meanwhile, the $NiSi_2$ peak shows an increase in intensity (Figure 8c), which indicates that Li

DOI: 10.1021/am506486w
ACS Appl. Mater. Interfaces 2015, 7, 1508–1515

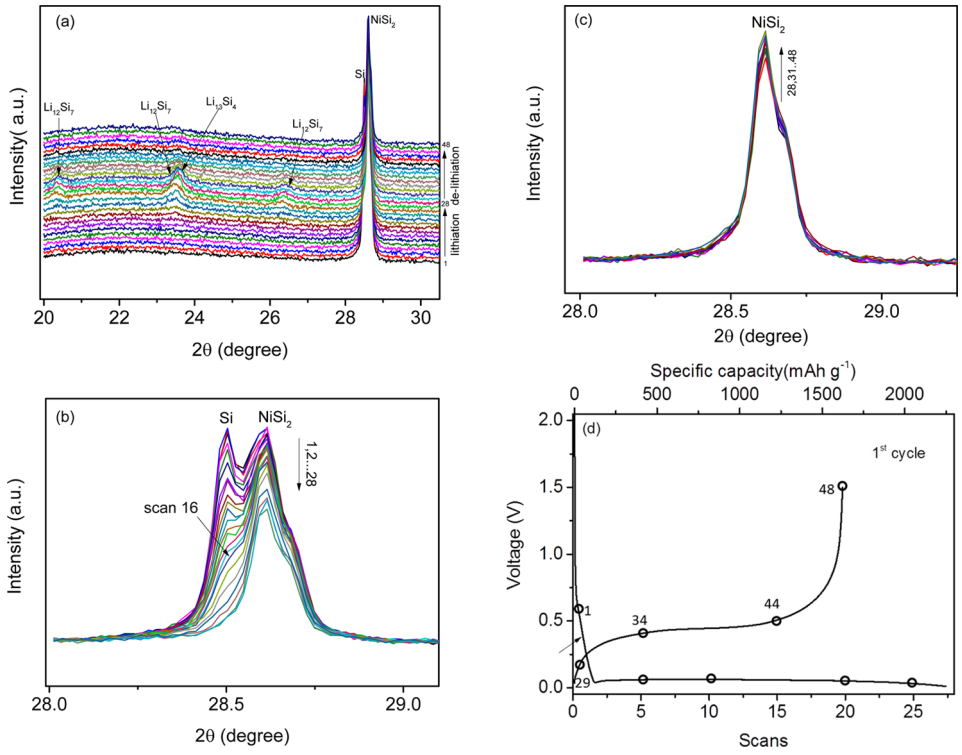

Figure 8. (a) Diagram showing the evolution of the XRD patterns upon lithiation and delithiation processes (scans 1−48) in a 2θ range of 20−32°. (b) Diagram indicating the evolution of the XRD patterns upon lithiation (scans 1−28) in a 2θ range of 28−29.2°. (c) Diagram indicating the evolution of the XRD patterns upon delithiation (scans 29−48) in a 2θ range of 28−29.2°. (d) Representative voltage vs specific capacity profile of the constant current discharge/charge cycling of the $NiSi_2$/Si/carbon composite anode at 0.05C (1st cycle) belonging to the in situ XRD measurement and displaying corresponding XRD scans.

insertion/extraction in $NiSi_2$ is partially reversible, thus proving that $NiSi_2$ can also partially react with Li^+. In the case of the $MeSi_x$ phase (e.g., FeSi,[36] $FeSi_2$,[23] and NiSi[37]), it is in general assumed that the silicide phase is irreversibly separated to silicon and metal and the element "Me" is inactive toward lithiation, while the silicon component reacts with lithium to form Li_xSi alloys during the first lithiation process ($xLi^+ + xe^- + MeSi \rightarrow Li_xSi + Me \leftrightarrows Me + Si + xLi^+ + xe^-$). Thus, the metal ("Me") will act as a buffering matrix for the formation of Li_xSi during subsequent cycling. However, Liu et al. presented a new and contradictory mechanism according to the results of an in situ XRD measurement, in which the NiSi phase can react reversibly with Li^+ to form Li_xNiSi as the lithiation process proceeds.[24] On the basis of our in situ XRD results, we also have faith in the assumption that the $NiSi_2$ phase in the composite is partially reversibly active to Li^+. Nevertheless, the exact role of the $NiSi_2$ phase in the composite during the lithiation/delithiation process remains unclear; thus, further studies are necessary to analyze its electrochemical behavior and Li^+ activity.

The charge/discharge cycling curves and Coulombic efficiency curves of the $NiSi_2$/Si/carbon composite as well as the rate performance of both the $NiSi_2$/Si and the $NiSi_2$/Si/carbon composites are illustrated in Figure 9a and 9b, respectively. The lithiation capacity slightly increases during the initial cycles, indicating the gradual improvement of the lithium extraction kinetics, which is most likely related to an increased wetting of the porous composite by the electrolyte (Figure 9a). The $NiSi_2$/Si/carbon material shows an excellent cycling stability with a high reversible capacity, even up to 200 cycles. The reversible capacity of the 200th cycle retains 1272

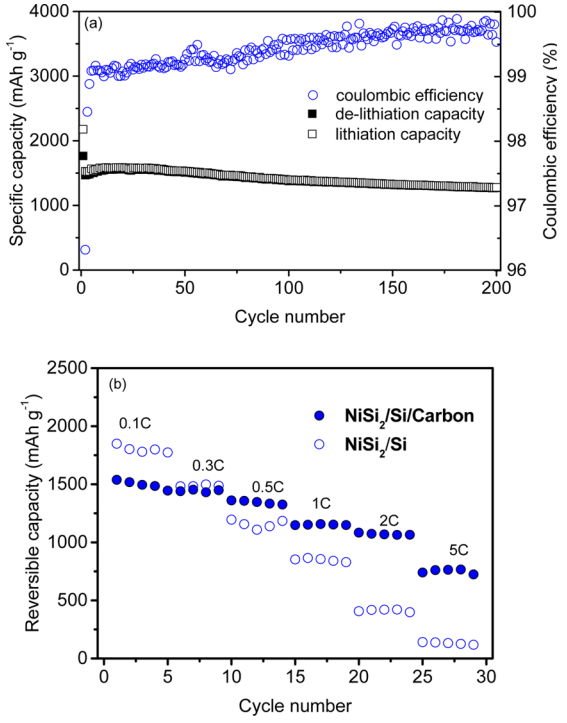

Figure 9. (a) Lithiation and delithiation capacity curves and Coulombic efficiency curves of the constant current cycling of $NiSi_2$/Si/carbon electrodes at 0.1C (1st cycle) and 1C (following cycles). (b) Reversible capacity curves of the $NiSi_2$/Si/carbon and $NiSi_2$/Si anode materials at different specific currents (C-rate investigation). Cut-off voltages for a and b are 0.01 and 1.5 V.

DOI: 10.1021/am506486w
ACS Appl. Mater. Interfaces 2015, 7, 1508−1515

mAh g^{-1}, with a capacity retention of 86.7% corresponding to the capacity of the second cycle (1467 mAh g^{-1}) and an average capacity fade rate of 0.07% per cycle. Meanwhile, after 10 cycles, the Coulombic efficiency exceeds 99% and keeps stable over 200 cycles. The superior cyclability of the $NiSi_2$/Si/carbon material can be most likely ascribed to the following reasons: (1) the porous structure offers sufficient void space to absorb the volume changes of silicon and (2) the $NiSi_2$ cores and carbon layer can not only effectively buffer the volume expansions of silicon but also maintain the conducting network of the electrode during ongoing cycling.

In particular, the $NiSi_2$/Si/carbon composite electrode exhibits an excellent rate performance. Figure 9b shows that the capacity reposefully declines from 1539 to 740 mAh g^{-1} when the current rate increases in stages from 0.1C to 5C (1C corresponds to a theoretical capacity of 2034 mAh g^{-1}). In the case of the pure $NiSi_2$/Si composite, the electrodes present a reatively poor rate capability at very high currents (i.e., above 1C), which, e.g., just gives a reversible capacity of 141 mAh g^{-1} at 5C. Obviously, the good rate capability of the $NiSi_2$/Si/carbon material benefits from the unique anode material structure with a high porosity, which decreases the pathways for ionic transport, and from the carbon coating layer enhancing the electronic conductivity.

4. CONCLUSION

In summary, a porous $NiSi_2$/Si/carbon composite with core−shell morphology was successfully prepared using a facile ball-milling method. The resulting $NiSi_2$/Si material demonstrated a porous structure and a homogeneous distribution of silicon crystallites with a size of about 20 nm, which are surrounding the surface of the $NiSi_2$ cores. The well-dispersed mesopores, having an average size of about 22 nm, and the $NiSi_2$ phase, which can be mainly considered as inactive component, serve as buffer zone to effectively accommodate the volume changes of silicon during lithiation/delithiation. After surface carbon coating by a CVD method, the as-prepared $NiSi_2$/Si/carbon composite displayed a stable specific capacity of 1272 mAh g^{-1} for 200 charge/discharge cycles at 1C and good rate capability with 740 mAh g^{-1} at a rate of 5C. In addition, the synthesis route developed in this work is very simple and low cost, using also cheap and abundant raw materials, which is in turn also possible to be used for the preparation of other silicon alloy composites with an improved cycling stability and rate performance.

AUTHOR INFORMATION

Corresponding Authors

*Phone: +49 251 83-36031. Fax: +49 251 83-36032. E-mail: martin.winter@uni-muenster.de.

*Phone: +49 251 83-36701. Fax: +49 251 83-36032. E-mail: tobiasplacke@uni-muenster.de.

Notes

The authors declare no competing financial interest.

ACKNOWLEDGMENTS

The authors thank the German Research Foundation for funding of this work in the project "WeNDeLIB" (Priority Programme 1473; Materials with New Design for Improved Lithium Ion Batteries). Furthermore, we gratefully acknowledge the supply of materials by Imerys Graphite & Carbon and Rockwood Lithium. We also thank Wei Wei from the Max Planck Institute (Polymer Research) for the constant support for TEM measurement.

REFERENCES

(1) Goodenough, J. B.; Kim, Y. Challenges for rechargeable batteries. *J. Power Sources* **2011**, *196* (16), 6688−6694.

(2) Armand, M.; Tarascon, J. M. Building better batteries. *Nature* **2008**, *451* (7179), 652−657.

(3) Wagner, R.; Preschitschek, N.; Passerini, S.; Leker, J.; Winter, M. Current research trends and prospects among the various materials and designs used in lithium-based batteries. *J. Appl. Electrochem.* **2013**, *43* (5), 481−496.

(4) Obrovac, M. N.; Christensen, L. Structural changes in silicon anodes during lithium insertion/extraction. *Electrochem. Solid State Lett.* **2004**, *7* (5), A93−A96.

(5) Hossain, S.; Kim, Y. K.; Saleh, Y.; Loutfy, R. Comparative studies of MCMB and C-C composite as anodes for lithium-ion battery systems. *J. Power Sources* **2003**, *114* (2), 264−276.

(6) Boukamp, B. A.; Lesh, G. C.; Huggins, R. A. All-Solid Lithium Electrodes with Mixed-Conductor Matrix. *J. Electrochem. Soc.* **1981**, *128* (4), 725−729.

(7) Winter, M.; Besenhard, J. O.; Spahr, M. E.; Novák, P. Insertion Electrode Materials for Rechargeable Lithium Batteries. *Adv. Mater.* **1998**, *10*, 725−763.

(8) Zhang, W. J. A review of the electrochemical performance of alloy anodes for lithium-ion batteries. *J. Power Sources* **2011**, *196* (1), 13−24.

(9) Winter, M. The Solid Electrolyte Interphase - The Most Important and the Least Understood Solid Electrolyte in Rechargeable Li Batteries. *J. Res. Phys. Chem. Chem. Phys.* **2009**, *223* (10−11), 1395−1406.

(10) Profatilova, I. A.; Stock, C.; Schmitz, A.; Passerini, S.; Winter, M. Enhanced thermal stability of a lithiated nano-silicon electrode by fluoroethylene carbonate and vinylene carbonate. *J. Power Sources* **2013**, *222*, 140−149.

(11) Profatilova, I. A.; Langer, T.; Badillo, J. P.; Schmitz, A.; Orthner, H.; Wiggers, H.; Passerini, S.; Winter, M. Thermally Induced Reactions between Lithiated Nano-Silicon Electrode and Electrolyte for Lithium-Ion Batteries. *J. Electrochem. Soc.* **2012**, *159* (5), A657−A663.

(12) Cui, L.-F.; Ruffo, R.; Chan, C. K.; Peng, H.; Cui, Y. Crystalline-Amorphous Core-Shell Silicon Nanowires for High Capacity and High Current Battery Electrodes. *Nano Lett.* **2009**, *9* (1), 491−495.

(13) Kim, H.; Seo, M.; Park, M. H.; Cho, J. A Critical Size of Silicon Nano-Anodes for Lithium Rechargeable Batteries. *Angew. Chem., Int. Ed.* **2010**, *49* (12), 2146−2149.

(14) Park, M. H.; Kim, M. G.; Joo, J.; Kim, K.; Kim, J.; Ahn, S.; Cui, Y.; Cho, J. Silicon Nanotube Battery Anodes. *Nano Lett.* **2009**, *9* (11), 3844−3847.

(15) Kim, H.; Han, B.; Choo, J.; Cho, J. Three-Dimensional Porous Silicon Particles for Use in High-Performance Lithium Secondary Batteries. *Angew. Chem., Int. Ed.* **2008**, *47* (52), 10151−10154.

(16) Yu, Y.; Gu, L.; Zhu, C.; Tsukimoto, S.; van Aken, P. A.; Maier, J. Reversible Storage of Lithium in Silver-Coated Three-Dimensional Macroporous Silicon. *Adv. Mater.* **2010**, *22* (20), 2247−2250.

(17) Ma, H.; Cheng, F.; Chen, J.; Zhao, J.; Li, C.; Tao, Z.; Liang, J. Nest-like silicon nanospheres for high-capacity lithium storage. *Adv. Mater.* **2007**, *19* (22), 4067−4070.

(18) Jia, H. P.; Gao, P. F.; Yang, J.; Wang, J. L.; Nuli, Y. N.; Yang, Z. Novel Three-Dimensional Mesoporous Silicon for High Power Lithium-Ion Battery Anode Material. *Adv. Energy Mater.* **2011**, *1* (6), 1036−1039.

(19) Yang, J.; Wang, B. F.; Wang, K.; Liu, Y.; Xie, J. Y.; Wen, Z. S. Si/C composites for high capacity lithium storage materials. *Electrochem.d Solid State Lett.* **2003**, *6* (8), A154−A156.

(20) Yoshio, M.; Wang, H. Y.; Fukuda, K.; Umeno, T.; Dimov, N.; Ogumi, Z. Carbon-coated Si as a lithium-ion battery anode material. *J. Electrochem. Soc.* **2002**, *149* (12), A1598−A1603.

DOI: 10.1021/am506486w
ACS Appl. Mater. Interfaces 2015, 7, 1508−1515

(21) Hu, Y. S.; Demir-Cakan, R.; Titirici, M. M.; Muller, J. O.; Schlogl, R.; Antonietti, M.; Maier, J. Superior storage performance of a Si@SiOx/C nanocomposite as anode material for lithium-ion batteries. *Angew. Chem., Int. Ed.* **2008**, *47* (9), 1645−1649.
(22) Liu, W.-R.; Yen, Y.-C.; Wu, H.-C.; Winter, M.; Wu, N.-L. Nanoporous SiO/carbon composite anode for lithium-ion batteries. *J. Appl. Electrochem.* **2009**, *39* (9), 1643−1649.
(23) Zhou, S.; Liu, X.; Wang, D. Si/$TiSi_2$ Heteronanostructures as High-Capacity Anode Material for Li Ion Batteries. *Nano Lett.* **2010**, *10* (3), 860−863.
(24) Liu, W.-R.; Wu, N.-L.; Shieh, D.-T.; Wu, H.-C.; Yang, M. H.; Korepp, C.; Besenhard, J. O.; Winter, M. Synthesis and characterization of nanoporous NiSi-Si composite anode for lithium-ion batteries. *J. Electrochem. Soc.* **2007**, *154*, A97−A102.
(25) Lee, H. Y.; Kim, Y. L.; Hong, M. K.; Lee, S. M. Carbon-coated $Ni_{20}Si_{80}$ alloy-graphite composite as an anode material for lithium-ion batteries. *J. Power Sources* **2005**, *141* (1), 159−162.
(26) Chen, Y.; Qian, J.; Cao, Y.; Yang, H.; Ai, X. Green Synthesis and Stable Li-Storage Performance of $FeSi_2$/Si@C Nanocomposite for Lithium-Ion Batteries. *ACS Appl. Mater. Interfaces* **2012**, *4* (7), 3753−3758.
(27) Fan, X.; Zhang, H.; Du, N.; Wu, P.; Xu, X.; Li, Y.; Yang, D. Vertically ordered Ni_3Si_2/Si nanorod arrays as anode materials for high-performance Li-ion batteries. *Nanoscale* **2012**, *4* (17), 5343−5347.
(28) Kim, T.; Park, S.; Oh, S. M. Preparation of core-shell Si/NiSi2/carbon composite and its application to lithium secondary batteries. *Electrochem. Commun.* **2006**, *8* (9), 1461−1467.
(29) Placke, T.; Schmuelling, G.; Kloepsch, R.; Meister, P.; Fromm, O.; Hilbig, P.; Meyer, H. W.; Winter, M. In situ X-ray Diffraction Studies of Cation and Anion Intercalation into Graphitic Carbons for Electrochemical Energy Storage Applications. *Z. Anorg. Allg. Chem.* **2014**, *640*, 1996−2006.
(30) Chianelli, R. R.; Scanlon, J. C.; Rao, B. M. L. Dynamic X-Ray Diffraction. *J. Electrochem. Soc.* **1978**, *125*, 1563−1566.
(31) Morcrette, M.; Chabre, Y.; Vaughan, G.; Amatucci, G.; Leriche, J. B.; Patoux, S.; Masquelier, C.; Tarascon, J. M. In situ X-ray diffraction techniques as a powerful tool to study battery electrode materials. *Electrochim. Acta* **2002**, *47* (19), 3137−3149.
(32) Liu, N.; Wu, H.; McDowell, M. T.; Yao, Y.; Wang, C.; Cui, Y. A Yolk-Shell Design for Stabilized and Scalable Li-Ion Battery Alloy Anodes. *Nano Lett.* **2012**, *12* (6), 3315−3321.
(33) Chan, C. K.; Peng, H. L.; Liu, G.; McIlwrath, K.; Zhang, X. F.; Huggins, R. A.; Cui, Y. High-performance lithium battery anodes using silicon nanowires. *Nat. Nanotechnol.* **2008**, *3* (1), 31−35.
(34) Green, M.; Fielder, E.; Scrosati, B.; Wachtler, M.; Serra Moreno, J. Structured silicon anodes for lithium battery applications. *Electrochem. Solid State Lett.* **2003**, *6* (5), A75−A79.
(35) Yen, Y.-C.; Chao, S.-C.; Wu, H.-C.; Wu, N.-L. Study on Solid-Electrolyte-Interphase of Si and C-Coated Si Electrodes in Lithium Cells. *J. Electrochem. Soc.* **2009**, *156* (2), A95−A102.
(36) Wang, G. X.; Sun, L.; Bradhurst, D. H.; Zhong, S.; Dou, S. X.; Liu, H. K. Innovative nanosize lithium storage alloys with silica as active centre. *J. Power Sources* **2000**, *88* (2), 278−281.
(37) Wang, G. X.; Sun, L.; Bradhurst, D. H.; Zhong, S.; Dou, S. X.; Liu, H. K. Nanocrystalline NiSi alloy as an anode material for lithium-ion batteries. *J. Alloys Compd.* **2000**, *306* (1−2), 249−252.

DOI: 10.1021/am506486w
ACS Appl. Mater. Interfaces 2015, 7, 1508−1515